ARMA 13-375

Modeling the Anisotropic Damaged Zone Around Hydraulic Fractures: Thermodynamic Framework and Simulation of Mechanical Tests

Xu, H. and Arson, C.
School of Civil and Environmental Engineering, Georgia Institute of Technology, Atlanta, Georgia, USA.
Damage Poro-Mechanics Lab, Georgia Institute of Technology, Atlanta, Georgia, USA.
Center for Tectonophysics, Texas A&M University, College Station, Texas, USA.
Busetti, S.
ConocoPhillips, Houston, Texas, USA.

ABSTRACT: We model crack propagation and damage induced by deviatoric stress around the crack tip. A new damage model is proposed to describe the damaged zone near fractures, in order to predict the mesoscale geomechanical behavior of rock during hydraulic fracturing. The process of new damage development follows a thermodynamic framework. An associated flow rule is utilized for irreversible strain rate while a non-associated flow rule is applied for damage evolution. Uniaxial tension and triaxial compression tests are simulated at the Gauss point of one element in MATLAB with the new damage model. The results illustrate the influence of anisotropic damage on stiffness degradation and residual strain development. The implementation of this new damage model in the commercial FEM software ABAQUS is undergoing. A preliminary Brazilian tension test is computed for the elastic domain using ABAQUS' UMAT subroutine. The result agrees well with the analytic solution. The new damage model for rock matches the theoretical expectations, and shows that the proposed model can predict anisotropic damage.

1. NUMERICAL MODELING OF HYDRAULIC FRACTURING

Hydraulic fracturing is a common technique used in tight hydrocarbon reservoirs to enhance native permeability and create conductive pathways back to the wellbore. To optimize the fluid injection parameters and assess resulting changes to production performance it is necessary to understand both the geometric dimensions and hydro-mechanical characteristics of the hydraulic fractures that are generated. Prediction of hydraulic fracturing requires coupling several theoretical frameworks, such as linear elastic fracture mechanics (LEFM), poro-mechanics and fluid mechanics. Because of the complex hydro-mechanical mechanisms involved, stress and deformation analyses cannot be determined straightforwardly and simplistic models are often used.

Classical models of hydraulic fracturing focus on stress concepts surrounding the borehole, and are based on the theory of elasticity [1-3]. The geometry of the borehole and the topology of the crack are assumed to be the dominant factors that operate within a generalized stress state. Based on the fracture geometry assumed, the "PKN", "KGD" and penny-shaped fracture models were proposed to describe idealized fracture propagation, and analytic solutions for these models were given [4-10]. With current FEM software available, more realistic hydraulic fracturing can now be modeled numerically at the reservoir scale. For instance, the "P3D" model was developed for layered problems. The material is divided into a series of small blocks on which hydraulic fracturing can be modeled [11]. An analytic solution for a penny-shaped fracture propagated by an incompressible Newtonian fluid flow was given by Savitski and Detournay [12], which based on the theory of lubrication. The stress intensity factor is considered in this elastic model. However, the coupling between mechanical equations and fluid flow was not mentioned. On the contrary, the planar 3D ("PL3D") model was formulated to predict the fracture footprint and the coupled fluid flow equation by a 2D mesh of cells. But the required CPU for the PL3D model was limiting [1].

The previous analytical solutions and numerical models do not consider degradation of stiffness and change in rock strength around the propagating fracture. However, it was established that hydraulic fracture propagation is

accompanied by the development of a damaged zone (made of cracks two to three orders of magnitude smaller than the hydraulic fracture) around the tip [13]. Without realistic prediction of how hydraulic fractures extend and propagate, companies risk making incorrect operational decisions, for example wells may be placed too close to other wells (interference) or natural features such as faults, or conversely, under-stimulation can leave valuable resource behind. Our aim here is to focus on improving the constitutive descriptions that are required to more realistically simulate hydraulic fracturing. To improve the prediction of rock stiffness in the damaged zone surrounding hydraulic fractures, an approach based on Continuum Damage Mechanics (CDM) is adopted in this work. Pressurization is expected to redistribute stress in the rock mass, and possibly change the principal directions and values of the stress tensor. That is the reason why in the proposed model, emphasis is put on the dependence of anisotropic crack propagation to differential stress. Previous damage models used in numerical simulation of hydraulic fracturing are limited to scalar damage. Models distinguishing between tension and compression [14] raise differentiability problems that are difficult to handle in numerical implementation. Multiple mechanisms are most often modeled by coupling damage and plastic potentials [15, 16], which tremendously increases the model complexity and the number of material parameters involved. Simpler models depend on empirical stress functions [13].

The outline of the new model is presented in Section 2. In Section 3, the principle of the tests simulated is presented in detail. MATLAB simulations (at the Gauss point) are performed to illustrate the development of anisotropic damage under uniaxial tension and triaxial compression. The model was programmed in ABAQUS UMAT, and a Brazilian test simulated in the elastic domain of UMAT (i.e. the damage model proposed was programmed in ABAQUS and used for this simulation, but the damage criterion was forced to remain negative in order to remain in the elastic domain). In Section 4, results are discussed and FEM predictions for the Brazilian test are compared to the theoretical solution of elasticity. Section 5 presents a methodology to calibrate the model parameters.

2. MODEL OUTLINE

The proposed model is purely phenomenological, i.e. it is based on postulates made on the form of energy potentials [17, 18]. The main postulates made in the proposed model are presented below.

2.1. Free Energy

The first assumption is the expression of the free energy of the solid skeleton. It is proposed to postulate a free energy potential expressed in stress (Gibbs free energy, G_s). The framework of hyper-elasticity is adopted, to ensure that the stiffness tensor derives from an elastic damaged potential [19]. The expression of the free energy should have quadratic terms in $\boldsymbol{\sigma}$ [20, 21]. In addition, it is usually assumed in CDM that G_s is linear in $\boldsymbol{D}$. The expression proposed in [21] is retained herein:

$$G_s(\boldsymbol{\sigma},\boldsymbol{D}) = \frac{1}{2}\boldsymbol{\sigma}:\mathbb{S}_0:\boldsymbol{\sigma} + a_1 Tr\boldsymbol{D}(Tr\boldsymbol{\sigma})^2 + a_2 Tr(\boldsymbol{\sigma}\cdot\boldsymbol{\sigma}\cdot\boldsymbol{D}) + a_3 Tr\boldsymbol{\sigma} Tr(\boldsymbol{D}\cdot\boldsymbol{\sigma}) + a_4 Tr\boldsymbol{D} Tr(\boldsymbol{\sigma}\cdot\boldsymbol{\sigma}) \quad (1)$$

In which $\mathbb{S}_0$ is the compliance of the intact material, in the absence of damage; $\boldsymbol{\sigma}$ is the stress tensor and $\boldsymbol{D}$ is damage tensor. The material parameters a_i need to be calibrated by numerical simulation (this will be discussed later in Section 4). The total elastic strain can be expressed from thermodynamic conjugation relationships:

$$\boldsymbol{\epsilon}^E = \boldsymbol{\epsilon} - \boldsymbol{\epsilon}^{id} = \frac{\partial G_s}{\partial \boldsymbol{\sigma}} = \frac{1+\nu_0}{E_0}\boldsymbol{\sigma} - \frac{\nu_0}{E_0}(Tr\boldsymbol{\sigma})\boldsymbol{\delta} + 2a_1(Tr\boldsymbol{D}\, Tr\boldsymbol{\sigma})\boldsymbol{\sigma} + a_2(\boldsymbol{\sigma}\cdot\boldsymbol{D} + \boldsymbol{D}\cdot\boldsymbol{\sigma}) + a_3[Tr(\boldsymbol{\sigma}\cdot\boldsymbol{D})\boldsymbol{\delta} + (Tr\boldsymbol{\sigma})\boldsymbol{D}] + 2a_4(Tr\boldsymbol{D})\boldsymbol{\sigma} \quad (2)$$

Where $\boldsymbol{\delta}$ is the second-order identity tensor, E_0 and ν_0 are Young's modulus and Poisson's ratio of the intact material, $\boldsymbol{\epsilon}^E$ is the total elastic strain. $\boldsymbol{\epsilon}$ is the total strain which is split into three terms, as illustrated in Fig. 1.

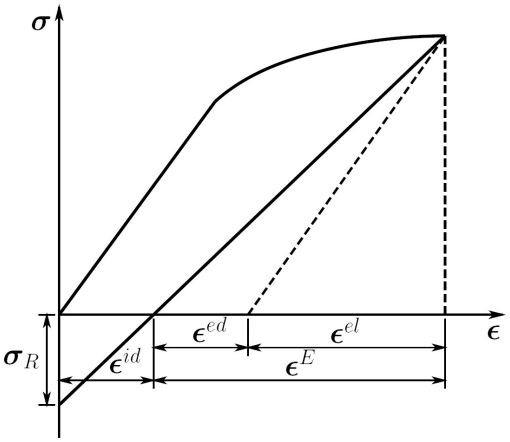

Fig. 1 Strain decomposition

In Fig. 1, $\boldsymbol{\epsilon}^{el}$ is the purely elastic deformation, and $\boldsymbol{\epsilon}^{ed}$ is the elastic damage-induced deformation due to the degradation of mechanical stiffness. The term $\boldsymbol{\epsilon}^{id}$ is introduced to account for the irreversible strain due to remaining crack openings induced by damage [22].

Similarly, from the expression of the free energy, the damage driving force $\boldsymbol{Y}$ conjugate to damage (or energy release rate) writes:

$$\boldsymbol{Y} = \frac{\partial G_s}{\partial \boldsymbol{D}} = a_1(Tr\boldsymbol{\sigma})^2 + a_2\boldsymbol{\sigma}\cdot\boldsymbol{\sigma} + a_3 Tr(\boldsymbol{\sigma})\boldsymbol{\sigma} + a_4 Tr(\boldsymbol{\sigma}\cdot\boldsymbol{\sigma})\boldsymbol{\delta} \quad (3)$$

2.2. *Damage Function*

The damage criterion is defined so as to : (1) capture both "crossing effects" and "splitting effects" under differential stress [23], and (2) model the difference of material behavior when the material is in tension or in compression. The damage criterion is modified from classic Drucker-Prager yield function by taking damage driving force instead of real stress:

$$f_d = \sqrt{J^*} - \alpha I^* - k \tag{4}$$

In which f_d is the damage function; α is the material parameter; J^* and I^* are defined as:

$$J^* = \frac{1}{2}\left(\mathbb{P}_1 : \boldsymbol{Y} - \frac{1}{3} I^* \boldsymbol{\delta}\right) : \left(\mathbb{P}_1 : \boldsymbol{Y} - \frac{1}{3} I^* \boldsymbol{\delta}\right) \tag{5}$$

$$I^* = (\mathbb{P}_1 : \boldsymbol{Y}) : \boldsymbol{\delta} \tag{6}$$

The projection tensor $\mathbb{P}_1$ ensures that the occurrence of damage be controled by the action of a tension damage driving force in the stress principal directions: it distinguishes tension and compression:

$$\mathbb{P}_1(\boldsymbol{\sigma}) = \sum_{p=1}^{3} \left[H\left(\boldsymbol{\sigma}^{(p)}\right) - H\left(-\boldsymbol{\sigma}^{(p)}\right)\right] \boldsymbol{n}^{(p)} \otimes \boldsymbol{n}^{(p)} \otimes \boldsymbol{n}^{(p)} \otimes \boldsymbol{n}^{(p)} \tag{7}$$

In which $H(\cdot)$ is the Heaviside distribution function, $\sigma^{(p)}$ is the pth eigenvalue of stress, and $\boldsymbol{n}^{(p)}$ is the corresponding eigenvector. The threshold k in Eq. (4) is a linear function of damage - which proved to reproduce well rock behavior [21, 24-26]:

$$k = C_0 - C_1 Tr(\boldsymbol{D}) \tag{8}$$

In which C_0 is the initial damage threshold, C_1 is the hardening variable for damage evolution. In $\mathbb{P}_1 : \boldsymbol{Y}$ space, the damage surface is a cone, similar to Drucker-Prager

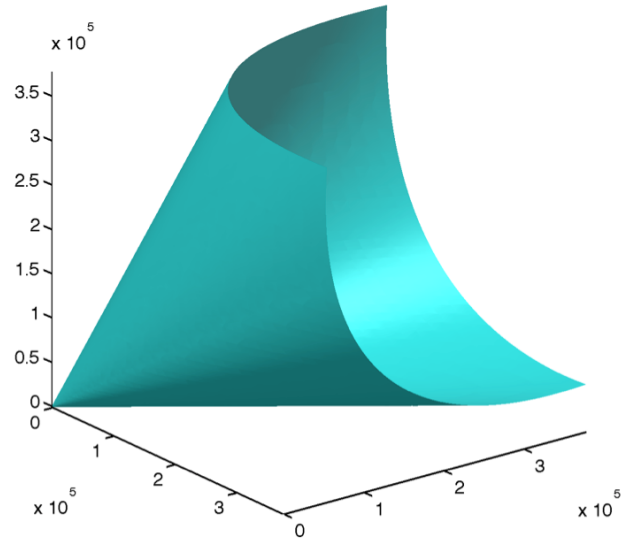

Fig. 2 Damage function in $\mathbb{P}_1 : \boldsymbol{Y}$ space

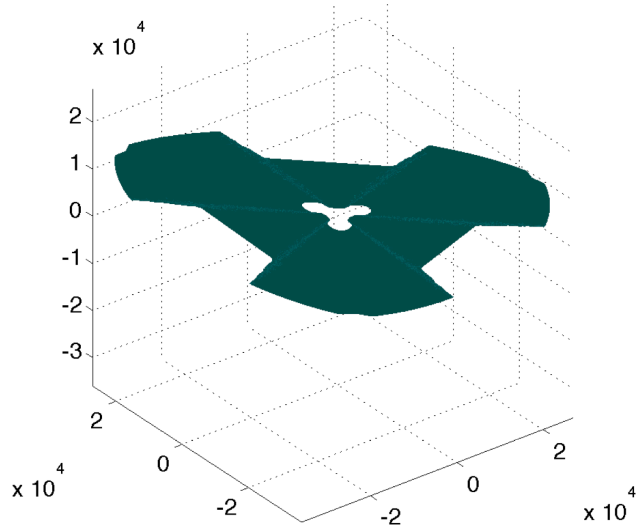

Fig. 3 Damage function in $\boldsymbol{Y}$ space

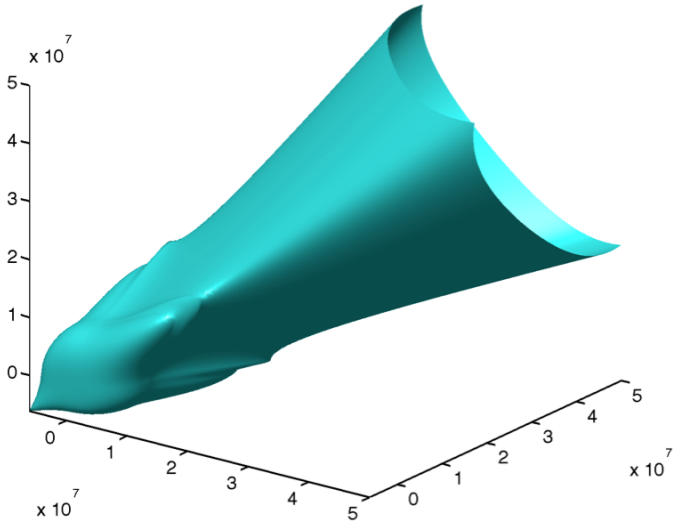

Fig. 4 Damage function in $\boldsymbol{\sigma}$ space

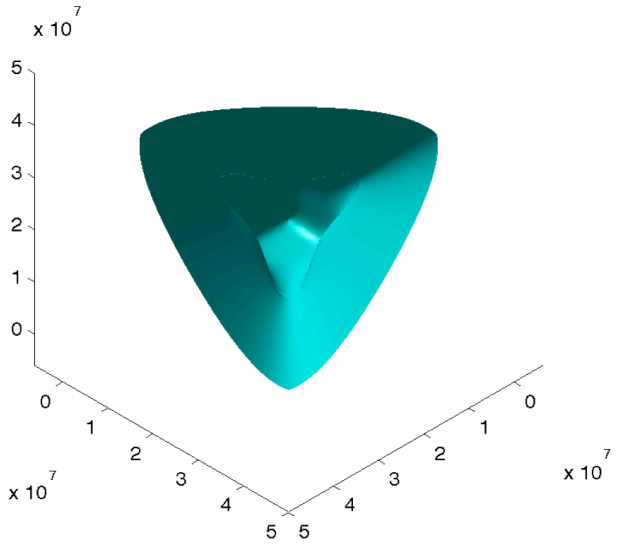

Fig. 5 Damage function in $\boldsymbol{\sigma}$ space

plasticity yield surface in stress space (Fig. 2). The plots show the damage surface in the space of the thermodynamic damage driving force $\boldsymbol{Y}$ (Fig. 3) and in stress space (Fig. 4 and 5). In fact the energy dissipation is load-path dependent. As a result, it is only locally positive. In zones where the surface is non-convex, the load path may cross the damage surface, and the predicted state of stress may fall outside the damage surface. Algorithms were proposed to solve the problem in numerical methods [27, 28].

2.3. Damage Potential

The model thermodynamic consistency is ensured if the reduced inequality of dissipation is satisfied. This condition is met as long as the increment of damage is positive for the current load step [29]. With the damage criterion proposed above, an associate flow rule could lead to some negative components of the rate of the dissipation variable, as illustrated in Fig. 6. The sign of the rate of dissipation depends on the location of the state of stress on the yield surface. To ensure the positivity of dissipation (and avoid getting negative damage increments), it is proposed to utilize a non-associate flow rule to predict damage evolution.

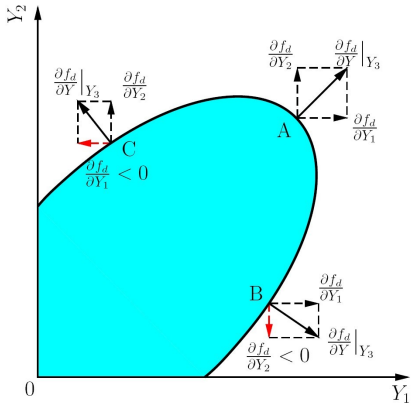

Fig. 6 If an associate flow rule were used, some components of the rate of damage would be negative.

The damage potential ($g_d \neq f_d$) is defined as a homogeneous function of degree one in $\boldsymbol{Y}$ [17, 30]:

$$g_d = \sqrt{\frac{1}{2}(\mathbb{P}_2 : \boldsymbol{Y}) : (\mathbb{P}_2 : \boldsymbol{Y})} - C_2 \qquad (9)$$

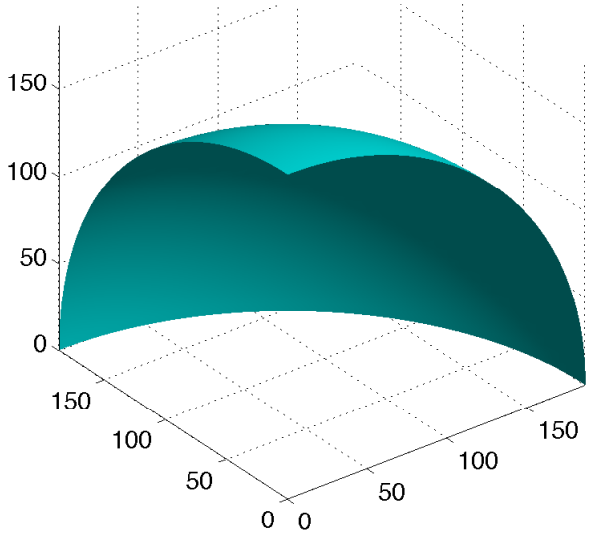

Fig. 7 Damage potential in $\mathbb{P}_2 : \boldsymbol{Y}$ space

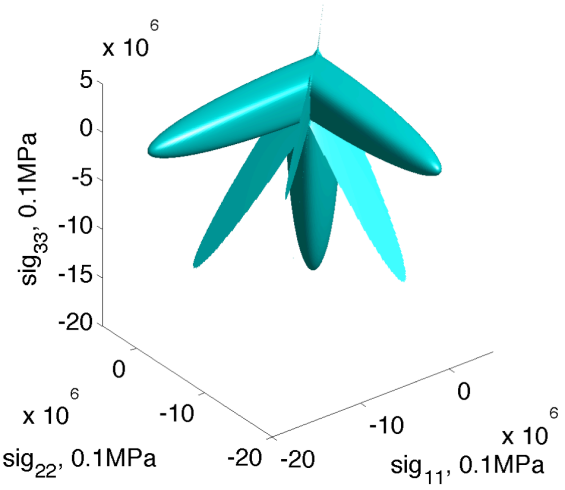

Fig. 8 Damage potential in $\boldsymbol{\sigma}$ space

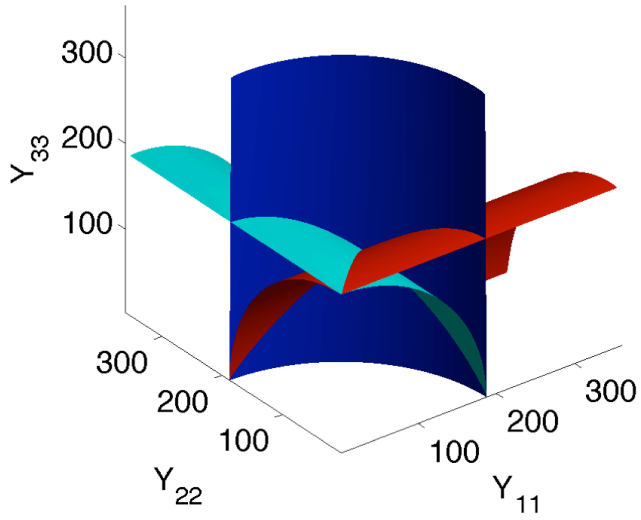

Fig. 9 Damage potential in $\boldsymbol{Y}$ space

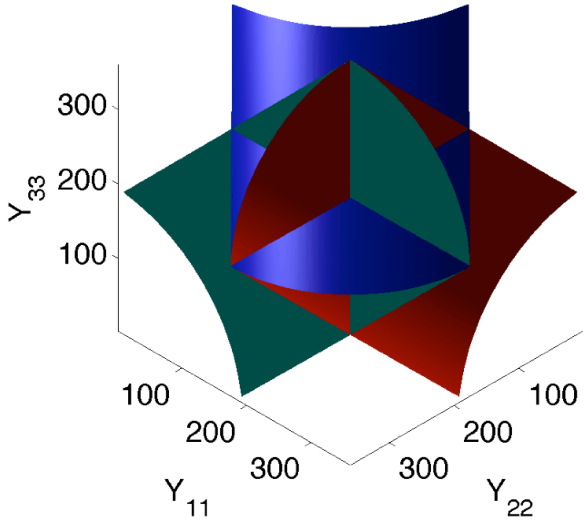

Fig. 10 Damage potential in $\boldsymbol{Y}$ space

In which C_2 is a parameter to locate the potential on the damage surface. The projection tensor $\mathbb{P}_2$ is introduced to ensure that the damage induced by deviatoric stress remains non-negative:

$$\mathbb{P}_2(\boldsymbol{\sigma}) = \sum_{p=1}^{3} H\left[\max_{q=1,2,3}(\boldsymbol{\sigma}^{(q)}) - \boldsymbol{\sigma}^{(p)}\right] \boldsymbol{n}^{(p)}\otimes\boldsymbol{n}^{(p)}\otimes\boldsymbol{n}^{(p)}\otimes\boldsymbol{n}^{(p)} \tag{10}$$

The function $\max(\cdot)$ is to choose the maximum value for a set of variables.

In the space of the physical damage driving force "$\mathbb{P}_2 : \boldsymbol{Y}$", the surface of the damage potential is an octant of a sphere (Fig. 7). Fig. 8 shows that the surface of the damage potential in stress space is composed of three closed surfaces (approximately cones). When two maximum principal stresses are equal, the state of stress lies on planes at the intersection between the cones.. The surface of the dissipation potential in the space of the components of $\boldsymbol{Y}$ is also composed of three surfaces. In Fig. 9 and 10, the three "branches" are shown with three different colors, to refer to the three possible cases (three possible maximum principal stresses). By construction, the state of stress can only lie on one branch at a time, except when two maximum principal stresses are equal. In the former case, the outward normal vector to the surface gives the direction of damage rate, which is indeed always non-negative. In the latter case, the normal direction at the intersection between two surfaces is not unique. However, a closed formulation exists to derive the damage rate (not detailed here), which ensures the thermodynamic and numerical consistency of the model. It is possible to calibrate the material parameters a_i in order to ensure the positiveness of the components of $\frac{\partial g_d}{\partial \boldsymbol{\sigma}}$ in numerical calculation, which is sufficient to ensure the local positivity of the damage rate and the thermodynamic consistency of the model (this issue is not discussed in detail in this article).

2.4. *Irreversible Deformation Flow Rule*

The last postulate required to close the formulation of the model is the flow rule for irreversible damage-induced deformation. If the damage potential defined above were used to predict the evolution of $\boldsymbol{\epsilon}^{id}$, the residual strain rate would remain parallel to the stress principal directions. However, it is expected that strains will develop perpendicular to crack planes, i.e. that $\boldsymbol{\epsilon}^{id}$ should have components orthogonal to stress directions. In order to get a reasonable (i.e. physical) prediction of deformation, an associate flow rule is utilized:

$$\dot{\boldsymbol{\epsilon}}^{id} = \dot{\lambda}_d \frac{\partial g_d}{\partial \boldsymbol{\sigma}} = \dot{\lambda}_d \frac{\partial g_d}{\partial \boldsymbol{Y}} : \frac{\partial \boldsymbol{Y}}{\partial \boldsymbol{\sigma}} \tag{11}$$

where $\dot{\lambda}_d$ is the Lagrangian multiplier which provides the magnitude of the irreversible strain.

3. SIMULATION OF MECHANICAL TESTS

Three classical laboratory tests are simulated with the new damage model. The two first are run at the Gauss point, within one element (with MATLAB), to verify the new damage model. The new model was also implemented in ABAQUS Finite Element software (UMAT subroutine), in order to solve boundary value problems. A Brazilian test is simulated with ABAQUS UMAT, in the elastic domain of the damage model, i.e. the damage criterion was forced to remain negative, in order to remain in the elastic domain. This preliminary implementation phase is useful to check the resolution algorithm in the Finite Element Method. The loading paths simulated are described below. Note that in the following sketches, the soil mechanics sign convention is adopted (i.e. tension counted negative, compression counted positive).

3.1. *Uniaxial tension*

The uniaxial tension test starts with a uniaxial tensile strain imposed on top and bottom of the element (Fig. 11). Then the strain is released to simulate unloading (Fig. 12).

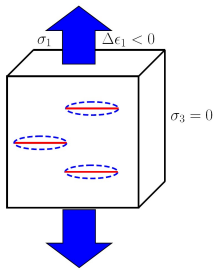

Fig. 11 Axial tension loading (O→B)

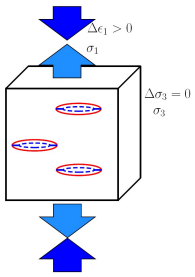

Fig. 12 Axial unloading (B→C)

According to the assumptions made in the proposed model, horizontal cracks will open due to tensile strain (Fig. 11). Then during the unloading process, the crack is expected to close – but not completely, since irreversible damage-induced deformation is expected. At the end of the test, the top and bottom surfaces will indeed be free of stress but with residual strain due to crack opening (Fig. 12).

3.2. *Triaxial compression*

Under triaxial compression, rock is cracking due to differential stress, which also called "compression damage". If there were some friction between the sample and the loading frame (Fig. 14), damage would initiate in the form of shear cracks. In practice, it is often assumed that friction at boundaries can be neglected, so that damage in compression initiates in the form of mode I Griffith cracks (parallel to the loading axis). Coalescence of Griffith cracks involves linkage of microscopic wing cracks (due to shear stress concentrations produced by rock heterogeneity). Clusters made of microscopic Griffith cracks linked together by wing cracks remain oriented parallel to the loading axis.

That is the reason why they are often considered as equivalent macroscopic Griffith cracks (opening under tensile boundary stress). This is known as the "crossing effect" [23].

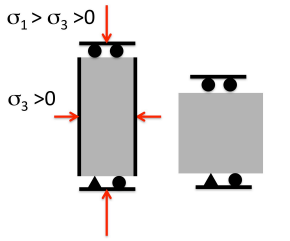

Fig. 13 Non frictional boundaries

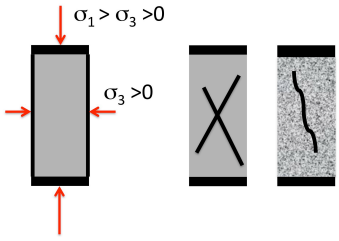

Fig. 14 Frictional boundaries

The loading phases in the triaxial compression simulation are: (1) isotropic compression (confining phase), (2) strain-controlled axial compression at constant confining pressure, (3) unloading. The main steps are illustrated in Fig.15-17.

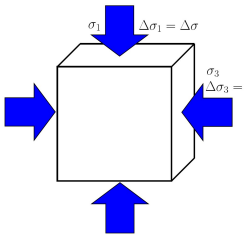

Fig. 15 (O→A) Isotropic compression

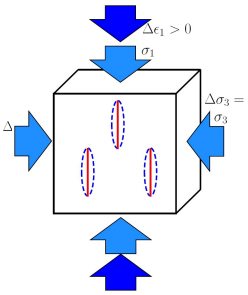

Fig. 16 (A→C) Axial loading

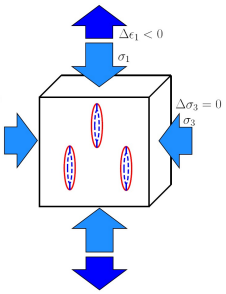

Fig. 17 (C→D) Axial unloading

3.3. *Brazilian test*

The Brazilian test is a type of indirect tension commonly used in rock mechanics. A cylindrical rock sample is subjected to a compressive force along its radial direction. This creates tensile stress at the center of the sample, along the loading direction. The elastic solution of the tensile is given as [31]:

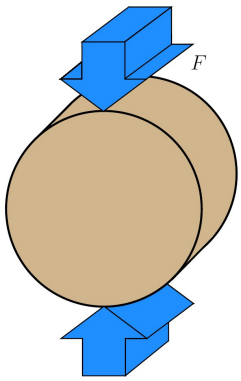

Fig. 18 Principle of the Brazilian test

$$\sigma_t = \frac{2F}{\pi dt} \tag{12}$$

In which F is the loading force; d and t are the diameter and thickness of the sample, respectively.

4. RESULTS AND DISCUSSIONS

The same type of rock was assumed in all simulations (a kind of granite [21]). The material parameters are given in Table 1. The simulations are to verify the model. Because the model are different (damage function and damage potential), even the same material parameters are used, the results cannot represent the same behavior of granite as the work done by Shao et al [21].

Table 1. Material parameters used in the simulation

E_0 GPa	ν_0	α	C_0 MPa	C_1 MPa
68	0.21	0.2309	0.001	0.55
a_1 $\times 10^{-4}$GPa	a_2 $\times 10^{-4}$GPa	a_3 $\times 10^{-4}$GPa	a_4 $\times 10^{-4}$GPa	-
1.2565	393.71	-12.565	2.513	-

4.1. *Uniaxial tension*

A vertical tensile strain $\epsilon_1 = -0.5\%$ is applied on the element. The damage is only obtained in the vertical direction ($D_1 > 0$), meaning that horizontal crack planes develop. As could be expected, irreversible strains are tensile in direction 1 ($\epsilon_1^{id} < 0$) and compressive in lateral directions ($\epsilon_2^{id} = \epsilon_3^{id} > 0$). Figs. 19-22 illustrate the results obtained: OA is the tension path in the elastic domain, and AB is the non-elastic tension phase (cracks propagate). The maximum tension stress during the test is -78.9 MPa: it corresponds to the maximum strain imposed in direction 1 (-0.5%). Damage accumulates only in direction 1 reaching $D1 = 35\%$. BC is the unloading step, in which ϵ_1 is relaxed. The model predicts that the damaged stiffness of the material is less than the original one. The residual stress observed after unloading proves that some irreversible deformation developed during the test. Damage remains constant during the unloading phase (constant vertical damage and zero lateral damage).

4.2. *Triaxial compression*

The first loading stage (OA) consists of imposing an isotropic confining pressure of 10MPa on the element. No damage is produced in the isotropic compression process (this loading phase was chosen far below the compressive limit). In a second stage, strain in direction 1 is increased by increments (up to 0.75%). Damage develops only in the horizontal directions (maximum $D_2 = D_3 = 65\%$ corresponding to the maximum deviatoric strain), while irreversible strains are compressive deformation in direction 1 ($\epsilon_1^{id} > 0$) and tensile deformation in lateral directions ($\epsilon_2^{id} = \epsilon_3^{id} < 0$). In this test, AB is the tension path in the elastic domain, and BC is the damaged compression phase (cracks propagate). The maximum deviatoric stress during the test is 235MPa, which is corresponding to the

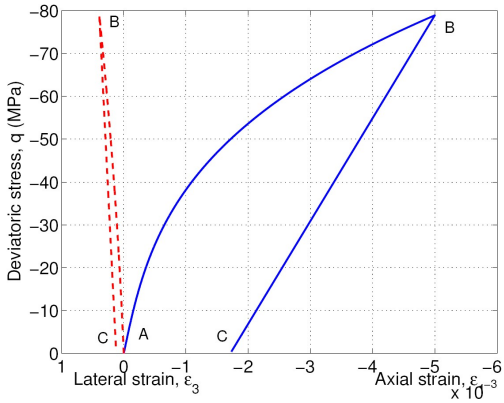

Fig. 19 Uniaxial tension test. Deviatoric stress versus axial strains.

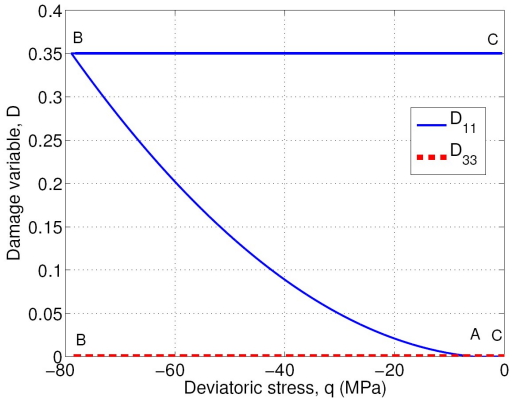

Fig. 20 Uniaxial tension test. Evolution of damage components with deviatoric stress.

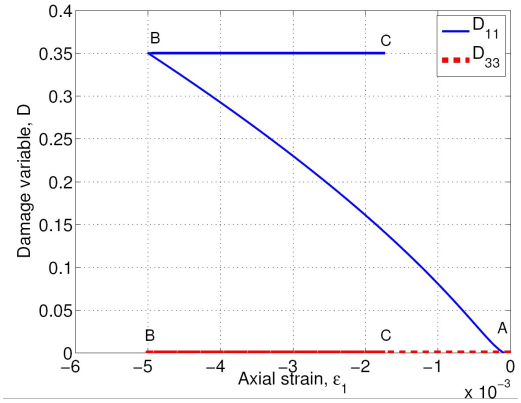

Fig. 21 Uniaxial tension test. Damage evolution with axial strain ϵ_1.

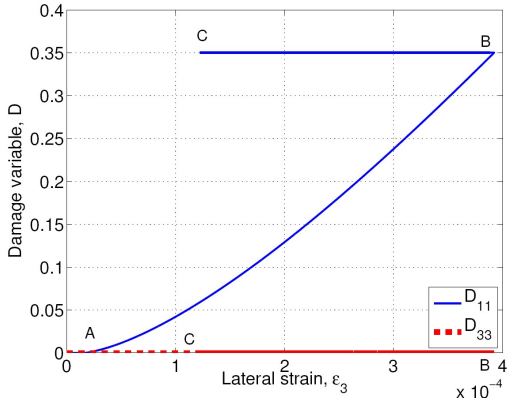

Fig. 22 Uniaxial tension test. Damage evolution with lateral strain ϵ_3.

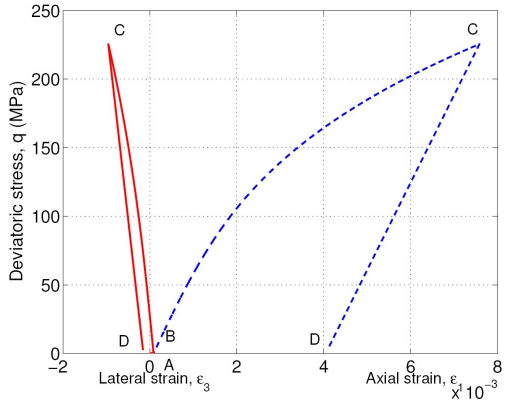

Fig. 23 Triaxial Compression Test. Deviatoric stress versus axial strains.

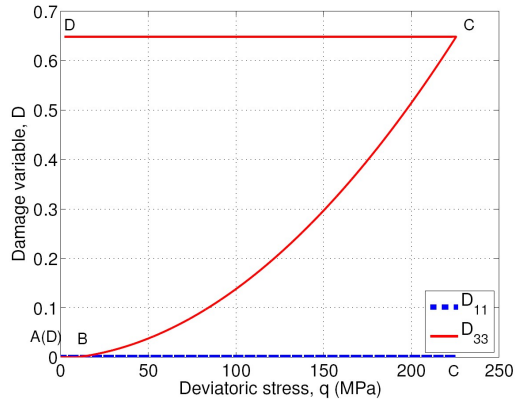

Fig. 24 Triaxial compression test. Evolution of damage components with deviatoric stress.

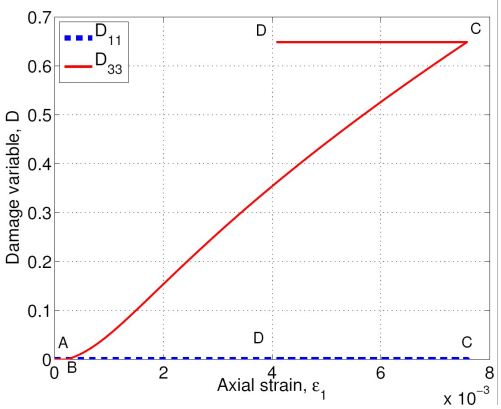

Fig. 25 Triaxial compression test. Damage evolution with axial strain ϵ_1.

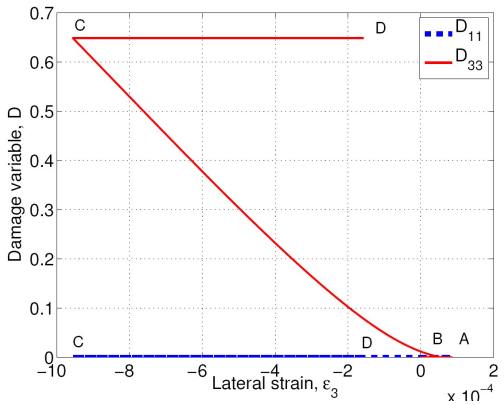

Fig. 26 Triaxial compression test. Damage evolution with lateral strainϵ_3.

maximum strain (0.75%) imposed in direction 1. ϵ_1 is relaxed in the unloading step (CD). The damaged stiffness of the material is less than the original one - which is shown as Fig. 23. Residual stress is also observed after unloading - like in the uniaxial tension test. Damage remains constant during the unloading phase: $D_2 = D_3$ (and still no damage occurs in vertical direction).

4.3. Brazilian test

This new damage model was implemented in a UMAT subroutine in ABAQUS Finite Element software, to allow full-scale simulations of hydraulic fracturing in the future. Developments are still on-going. In the following, results constrained in the elastic domain of the damage model are presented and discussed for a Brazilian test. The algorithm is validated against an analytic solution developed in elasticity.

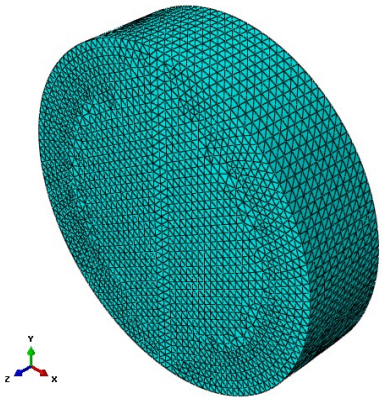

Fig. 27 Mesh of Brazilian test

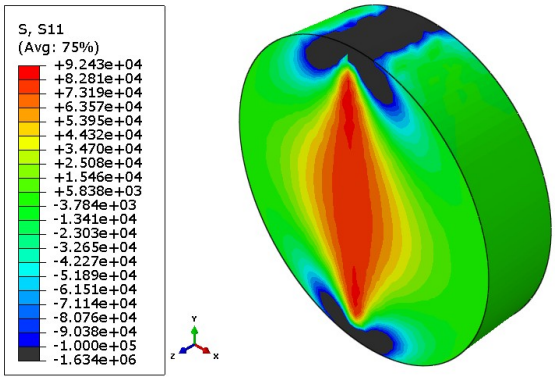

Fig. 28 Distribution of horizontal tensile stress $\boldsymbol{\sigma_1}$ obtained with the FEM in the elastic domain of the damage model.

The mesh adopted is shown in Fig. 27. Elements used for this simulation are linear tetrahedrons which allows a good fit to the sample geometry, but provides less accurate results than hexahedral elements. A force of 1260 N is imposed on a very narrow surface at top of the sample, so that it can be treated as line load. According to the theory of elasticity, when a line load is applied on the top of the sample, a uniform horizontal tensile stress is distributed along the diameter in the middle of rock sample, except in the region very close to the load point (in fact, the analytical solution near the load point gives an infinite stress). The numerical results obtained in the elastic domain with UMAT are shown in Fig. 28. Horizontal stress is predicted in the middle of the sample, and not close to the loading points, which is in agreement with the theoretical solution. However, stress distribution is not uniform along the diameter of the sample. The analytical solution provided by Eq. 12 ($\sigma_t = 80.3\,\text{kPa}$) is based on 2-D calculation. In the present 3-D simulation, the result for tensile stress along the diameter of the sample is $\sigma_t \approx 80\sim82\text{kPa}$.

5. RATIONALE TO CALIBRATE MODEL PARAMETERS

Since the damage criterion accounts for stress-induced propagation modes (compression and tension), it is necessary to calibrate the model both in compression and in tension. In this paper, we presented a uniaxial compression test and a uniaxial tension test. Each experiment performed for model calibration should include at least one loading step with damage-induced reduction of stiffness, and one unloading step (until the state of free stress). The very beginning of linear elastic loading path can be used to determine the elastic parameters: undamaged Poisson's ratio (ν_0) and Young's modulus (E_0). The damaged Poisson's ratio (i.e. ν_{13}) and Young's modulus (E_1) can be calibrated from the unloading slope.

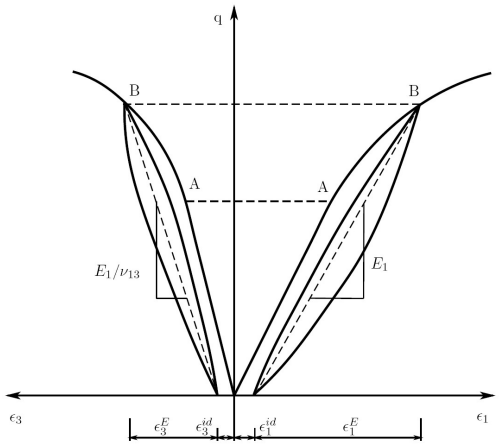

Fig. 29 Deviatoric Loading Step for Triaxial Compression [24]

The initiation of damage starts from point A (Fig. 29), where the threshold reached in the damage criterion can be calculated:

$$J^*(\boldsymbol{\sigma}_A) - \alpha I^*(\boldsymbol{\sigma}_A) - C_0 = 0 \qquad (13)$$

Point B of the damaged state (Fig. 29) will give a second equation for the damage criterion:

$$J^*(\boldsymbol{\sigma}_B) - \alpha I^*(\boldsymbol{\sigma}_B) - C_0 - 2C_1\boldsymbol{D}_B = 0 \qquad (14)$$

5.1. Uniaxial Tension

For the uniaxial compression test, the model proposed assumes that damage will only develop in the direction

of the tensile loading axis, so $D_2 = D_3 = 0$. After some computations:

$$E_1 = \frac{1}{\frac{1}{E_0}+2(a_1+a_2+a_3+a_4)D_1} \quad (15)$$

$$\frac{E_1}{\nu_{13}} = \frac{1}{\frac{\nu_0}{E_0}-2a_1D_1-a_3D_1} \quad (16)$$

Another loading/unloading cycle will provide two damage points A' and B', similar to A and B above, which will give two more equations for parameters.

5.2. Uniaxial Compression

In the uniaxial compression test, the proposed model provides $D_1 = 0$. Moreover, due to the axis-symmetric conditions, $D_2 = D_3$. In the unloading step, $\sigma_1 = q$, and $\sigma_2 = \sigma_3 = 0$. After some computations:

$$E_1 = \frac{1}{\frac{1}{E_0}+4a_{1D_3}+4a_4D_3} \quad (17)$$

$$\frac{E_1}{\nu_{13}} = \frac{1}{\frac{\nu_0}{E_0}-4a_1D_3-a_3D_3} \quad (18)$$

The damage criterion calculated at point A (Eq. 13) and at point B (Eq. 14) provides two more equations. As a conclusion, based on the analysis above, we have 4 independent equations for the uniaxial compression test and 4 independent equations for the uniaxial tension test. We have 7 material parameters to determine in the proposed damage model (a_1, a_2, a_3, a_4, C_0, C_1, α) plus 2 unknowns (D_3 for the uniaxial compression test and D_1 for uniaxial tension test), 9 parameters in total. There is one equation missing. Increasing the number of tests does not provide more equations, because each test will also add one unknown (D_3 for the uniaxial compression test and D_1 for uniaxial tension test). This means that the model can only be calibrated by an iterative process: we need to assume an initial value for either D_3 or D_1 and do an iterative calculation of the damaged stiffness tensor. The flow rule (Eq. 11) for each test is calculated in the iterative process. Experimental stress/strain curves can be used to define objective functions. Calibration is performed by ensuring that the difference between the experimental results and the model prediction satisfies a convergence criterion given *a priori*.

6. CONCLUSION

A Continuum Damage Mechanics (CDM) model is developed to predict anisotropic damage induced by differential stress around hydraulic fractures. The proposed damage model captures both splitting and crossing effects due to deviatoric stress, and has different damage thresholds in tension and compression. In order to relate damage evolution to differential stress, a damage criterion similar to Drucker-Prager yield function is defined - but it is expressed in terms of a damage driving force instead of stress. To ensure the positivity of dissipation, a non-associated flow rule is utilized for the damage evolution law. An associated flow rule is employed for the irreversible strain in order to capture deformation induced by residual crack opening. The damage increment is computed by deriving potentials from the total force conjugate to damage – not from an absolute value of a part of force component. Within this framework, new damage model meets thermodynamic requirements, follows a rigorous formulation and allows physically consistent predictions of damage, deformation and stiffness.

A uniaxial tension test and a triaxial compression test have been simulated at the Gauss point with MATLAB. The model captures well the propagation of crack planes in the direction parallel to major compression stress, and the subsequent anisotropy induced on stiffness and deformation. In addition, the damage criterion allows distinguishing between crack propagation in tension and compression.

A Brazilian test has been simulated with the Finite Element Method in the elastic domain of the damaged model. Predictions are in reasonable agreement with the theoretical elastic solution. Discrepancies are attributed to numerical errors associated to the choice of interpolation functions.

The damage model requires 7 material parameters. An iterative calibration procedure has been explained in order to determine these model parameters from uniaxial tension tests and triaxial compression tests.

In its present form, the model is sensitive to material parameters. The next step of this research work will be model validation and calibration against real experimental data. The proposed model is expected to give useful insights for the formulation of new constitutive models for rock and concrete. It is also the first step towards the development of a framework allowing modeling multi-scale crack propagation. Further modeling work will be dedicated to hydro-mechanical couplings during fluid injection, in order to track porosity and permeability changes induced by damage.

ACKNOWLEDGEMENTS

This research was performed in the School of Civil and Environmental Engineering at the Georgia Institute of Technology, with the support of ConocoPhillips on a project entitled “Finite Element Modeling of Hydraulic Fracturing”.

REFERENCES

1. Whittaker, B. N., R. N. Singh and G. Sun. 1992. *Rock fracture mehcanics: principles, design, and application*.

Elsevier.

2. Abou-Sayed, A. S..1978. An experimental technique for measuring the fracture toughness of rocks under downhole stress condition. *VDI-Berichte.* 313: 829-824.
3. Winter, R. B. and F. Rummel, 1982. Application of laboratory fracture mechanics data to hydraulic fracturing field tests. In *Proceedings of 1st japan-USA Symp. on Fracture Mechanics Approach, Hydraulic fracture and Geothermal Energy*.
4. Perkins, T. K. and L. R. Kern. 1961. Widths of hydraulic fractures. *J. Pet. Tech.*. 13(9): 937-949.
5. Sneddon, I. N. and H. A. Elliot. 1946. The opening of a griffith crack under internal pressure. *Q. Appl. Math.. 4:* 262-267.
6. Nordren, R. P.. 1972. Propagation of a vertical hydraulic fracture. *SPE. J.*. 12(8): 306-314.
7. Khristianovic , S. A. and Y. P. Zheltov. 1955. Formation of vertical fractures by means of highly viscous liquid. In *Proceedings of the fourth world petroleum congress*.
8. Geertsma, J. and F. de Klerk. 1969. A rapid method of predicting width and extent of hydraulically induced fractures. *J. Pet. Tech.*. 21: 1571-1581.
9. Sneddon, I. N.. 1946. The distribution of stress in the neighbourhood of a crack in an elastic solid. In *Proceedings of R. Soc. London A.*.
10. Sneddon, I. N. and A. E. Green. 1950. The distribution of stress in the neighbourhood of a flat elliptical crack in an elastic solid. In *Proceedings of Cambridge Philos. Soc.*.
11. Mack, M. G. and N. R. Warpinski. 2000. *Mechanics of hydraulic fracturing. In: Economides, Nolte, editors. Reservoir stimulation.* Chichester; Wiley.
12. Savitski, A. and E. Detournay. 2002. Propagation of a penny-shaped fluid-driven fracture in an impermeable rock: asymptotic solutions. *International Journal of Solids and Structures.* 39: 6311-6337.
13. Valko, P. and M. J. Economides. 1994. Propagation of Hydraulically Induced Fractures a Continuum Damage Mechanics Approach. *International Journal of Rock Mechanics and Mining Sciences & Geomechanics Abstracts*. 31: 221-229.
14. Mazars, J.. 1986. A description of micro- and macro scale damage of concrete structures. *J. Eng. Mech.*. 115: 345-365.
15. Lubliner, J., J. Oliver, S. Oller and E. Onate. 1989. A Platic-Damage model for Concrete. *International Journal of Solids and Structures.* 23: 299-326.
16. Lee, J. and G. Fenves. 1998. Plastic-damage model for cyclic loading of concrete structure. *Journal of Engineering Mechanics.* 124: 892-900.
17. Collins, I. F. and G. T. Houlsby. 1997. Application of Thermomechanical Principles to the Modelling of Geotechnical Materials. In *Proceedings: Mathematical, Physical and Engineering Sciences*. 453: 1975-2001.
18. Rice, J. R.. 1968. 3 of Fracture: An Advanced Treatise. In *Mathematical Analysis in the Mechanics of Fracture.* ed.
19. H. Liebowitz, 191-311
    Houlsby, G. T. and A. M. Puzrin. 2006. *Principles of hyperplasticity an approach to plasticity theory based on thermodynamic principles.* London: Springer.
20. Halm, D. and A. Dragon. 1998. An anisotropic model of damage and frictional sliding for brittle materials. *Eur. J. Mech. A/Solids*. 17: 439-460.
21. Shao, J. F., H. Zhou and K. T. Chau. 2005. Coupling between anisotropic damage and permeability variation in brittle rocks. *International Journal for Numerical and Analytical Methods in Geomechanics*. 29(12): 1231-1247.
22. Abu Al-Rub, R. and G. Z. Voyiadjis. 2003. On the coupling of anisotropic damage and plasticity models for ductile materials. *International Journal of Solids and Structures*. 40: 2611-2643.
23. Ortiz, M. 1985. A constitutive theory for the inelastic behaviour of concrete. *Mech. Mater.*. 4: 67-93.
24. Halm, D. and A. Dragon. 2002. Modelisation de l'endommagement par mesofissuration du granite. *Revue Francaise de Genie Civi*. 17: 21-33.
25. Homand-Etienne, F., D. Hoxha and J. F. Shao. 1998. A continuum damage constitutive law for brittle rocks. *Computers and Gotechnics*. 22: 135-151.
26. Shao, J. F., K. T. Chau and X. T. Feng. 2005. Modeling of anisotropic damage and creep deformation in brittle rocks. *International Journal of Rock Mechanics & Mining Sciences*. 43: 582-592.
27. Carstensen, C., K. Hackl and A. Mielke. 2002. Non-convex potentials and microstructures in finite-strain plasticity. *Royal Society of London Proceedings Series A*. 458(2018): 299-317.
28. Pedroso, D. M., D. Sheng and S. W. Sloan. 2008. Stress update algorithm for elastoplastic models with nonconvex yield surfaces. *International Journal for Numerical Methods in Engineering*. 76: 2029-2062.
29. Desmorat, R.. 2006. Positivite de la dissipation intrinseque d'une classe de modeles d'endommagement anisotropes non standards. *Comptes Rendus Mecanique*.
30. Senseny, P. E., F. D. Hansen, J. E. Russell, N. L. Carter and J. W. Handin. 1992. Mechanical behaviour of rock salt: Phenomenology and micromechanisms. *International Journal of Rock Mechanics and Mining Sciences &*
31. *Geomechanics Abstracts*. 29: 363-378.
    Goodman, R. E.. 1989. *Introduction to Rock Mechanics*. Wiley.
32. Zoback, M. D. and D. D. Pollard. 1978. Hydraulic fracture propagation and the invterpretation of pressure-time records for in site dterminations. In *Proceedings of 19th U.S. Symp. on Rock Mech*.
33. Sih, G. C. and H. Liebowitz. 1968. Mathematical theories of brittle fracture. In *Proceedings of Fracture, An advanced Treatise*.